Journal of Solid Mechanics Vol. 9, No. 1 (2017) pp. 126-137

Comparison of Stiffness and Failure Behavior of the Laminated Grid and Orthogrid Plates

A. Ehsani , J. Rezaeepazhand *

Department of Mechanical Engineering, Ferdowsi University of Mashhad, Mashhad, Iran

Received 8 November 2016; accepted 6 January 2017

ABSTRACT

The present paper investigates the advantages of a new class of composite grid structures over conventional grids. Thus far, a known grid structure such as orthogrid or isogrid has been used as an orthotropic layer with at most in-plane anisotropy. The present laminated grid is composed of various numbers of thin composite grid layers. The stiffness of the structure can be adjusted by choosing proper stacking sequences. This concept yields to a large variety of laminated grid configurations with different coupling effects compare to conventional grids. To illustrate the advantages of the laminated grids, the stiffness matrices and the bending response of the laminated and conventional grids are compared. Furthermore, a progressive failure analysis is implemented to compare the failure resistance of laminated and conventional grids. The results indicate that, thoughtful selection of stacking sequences of the laminated grid enhances the stiffness and response of the laminated grids without significant effect on the failure index.

Keywords : Laminated grid; Composite; Stiffness; Orthogrid; Plate bending; Progressive failure.

1 INTRODUCTION

THE grid structures can be designed to endure specific loads in particular directions. This benefit can reduce the weight of structures [1]. The grid structures are extensively used in aerospace, civil, and marine structures. Grid structures are usually made from metals, woods and composite materials. Due to exceptional properties of the reinforced composite materials, low weight, directional and tailor able properties, they are widely used in high performance structures such as grids.

Nearly all studies in the field of grid structures have been focused on the developing the model, optimization of the patterns and buckling, bending and vibration response of a single layer composite grid structure. Chen and Tsai [2] presented an integrated equivalent stiffness model to represent a grid with or without skin. They illustrated a method of designing an optimum grid structure under multiple loads. Gurdal and Gendron [3] evaluated the structural efficiency of geodesically stiffened shells with various stiffener arrangements under compression, torsion and combined loads. Similarly, in an optimization process, Oliveira and Christopoulos [4] presented a practical method of finding a minimum weight of grid plates subjected to a lateral load. Kidane et al. [5] used the smeared method to analysis buckling of the grid stiffened shell, and validated the results with experimental results. Ambur and Jaunky [6] developed an optimal design strategy for grid structures with variable curvatures for global and local buckling analysis. Moreover, Chen et al. [7] presented spline compound stripe method to analysis the free vibration of a stiffened plate. Their results were in good agreement with the experimental and numerical results. Shi et al.[8] presented an equivalent stiffness model considering a non-uniform grid distribution. Their model has been used to

*Corresponding author. Tel.: +98 513 880 5123.
E-mail address: jrezaeep@um.ac.ir (J. Rezaeepazhand).

calculation the critical buckling loads of advanced grid-stiffened conical shells under uniform external pressure. They showed good agreement between the predictions of their model and experimental and numerical simulations.
Lai et al. [9] studied the buckling behavior and structural efficiency of six typical composite grid cylindrical shells under axial compression, pure bending, transverse bending and torsion by parameterized finite element models. They also investigated the effects of the grid patterns and the helical angles on the buckling strength and buckling mode shapes of the structures. Huang et al. [10] present a new finite element modeling technique to calculate the buckling response of different types of grid stiffened structures. Their modeling strategy, reduce the number of unknowns compared to the conventional approaches. They also investigate the buckling load capacity of different type of grid stiffened structures. They indicated skin thickness, stiffener width and thickness have significant effects on the improvement of buckling resistance of these panels.

Anyfantis et al. [11] used the progressive failure analysis to predict the post buckling progressive and final failure of T-stiffened plat. They used Hashin and Tsai-Wu failure criteria and showed their results are in good agreement with published results. In similar work, Pietropaoli [12] investigated the progressive failure on two types of composite structures, a specimen with a hole and an I-stiffened panel, under in-plane compression load. The results show good agreement with experimental results.

Although, the conventional composite grid structures have been extensively studied in the recent years, there has not been any attention to the laminated grid structures. Similar to laminated composites, variety of laminated grid structures can be created using different grid types with various stacking sequences (see Fig. 1). Tailored stiffness of the structure is achieved by using full anisotropic properties of the laminated grid compare to orthotropic properties with at most in-plane anisotropic of the conventional grid.

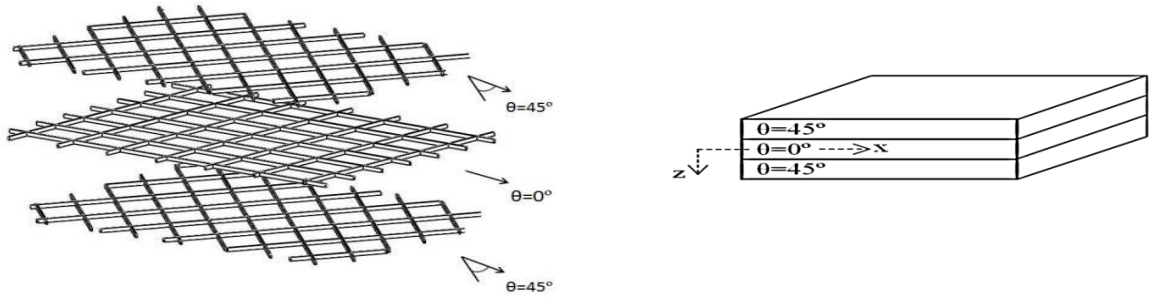

Fig.1
Assembly of three conventional orthogrid layers into (45/0/45) laminated grid.

In the present study, the concept of the laminated grid structures is introduced, and its advantages over conventional grids are investigated. To show the advantages of the laminated grid structures over conventional grids, different symmetric angle ply laminated grids are considered. Using laminated plate theory, the stiffness matrices of the laminated grid plates are obtained. The extensional and bending stiffness matrices and the deflection of the laminated grid plates are calculated.

To illustrate the effect of lamination on the stiffness of the structures, variations of the coupling and summation of the elements of the stiffness matrices are calculated. Moreover, two non-dimensional parameters, which express the closeness of a laminated structure to its equivalent orthotropic layer, are also used. The results are compared with corresponding results for conventional orthogrids. It is assumed that, a laminated grid is constructed by stacking a specific number of perfectly bonded thin elastic grid layers.

As shown in Fig.1, due to angular position of the two adjacent grid layers, the contact areas between the layers in the laminated grids are less than conventional grids. So, to evaluate the failure behavior of the laminated grids, the USDFLD subroutine in ABAQUS software is applied to investigate the progressive failure of the plates. Three principal failure modes, namely, matrix failure, fiber-matrix shear failure and fiber failure are studied and compared in the plates. Eventually, the failure analysis results have been compared to ensure the reduction in the contact area, will not significantly affect the failure of the laminated grid structures.

2 LAMINATED GRID STRUCTURES

Similar to a laminated composite, several layers of different type of grids with various thickness and orientations can constitute a laminated grid. In this study, the laminated grids are consisting of orthogrid layers in which the principal

grid directions are not necessarily paralleled to the plate axes. As an example, Fig. 1 illustrates a three layers laminated grid with (45º/0º/45º) stacking sequence.

To obtain the stiffness matrices of a laminated grid plate, the classical laminated plate theory is used. Similar to laminated plates, the extensional, coupling and bending stiffness matrices of the laminated grid are as follows [13]:

$$\begin{aligned} A_{ij} &= \sum_{K=1}^{N} \left(\overline{Q}_{ij}\right)_k \left(z_k - z_{k-1}\right) \\ B_{ij} &= \frac{1}{2} \sum_{K=1}^{N} \left(\overline{Q}_{ij}\right)_k \left(z_k^2 - z_{k-1}^2\right) \\ D_{ij} &= \frac{1}{3} \sum_{K=1}^{N} \left(\overline{Q}_{ij}\right)_k \left(z_k^3 - z_{k-1}^3\right) \end{aligned} \tag{1}$$

where, k is the layer number in the laminate, Z_k is distance of k layer from the middle surface, and N is the number of the grid layers. For simplicity, it is assumed the present laminated grids are symmetric; consequently, the coupling stiffness matrix $[B]$ is vanished. To calculate the stiffness matrices of a laminated grid, the transformed reduced stiffness matrices, $[\bar{Q}]$, of each grid layer are needed. The equivalent stiffness model (ESM) is applied to calculate the reduced stiffness matrices of the orthogrid layer [2]. Eq. (2) presents the reduced stiffness matrix, $[Q]$, of a conventional orthogrid layer [2].

$$[Q] = \begin{bmatrix} \frac{E_1 t_1}{d_1} & 0 & 0 \\ 0 & \frac{E_1 t_2}{d_2} & 0 \\ 0 & 0 & \frac{G_{12} t_1}{d_1} + \frac{G_{12} t_2}{d_2} \end{bmatrix} \tag{2}$$

d_1, d_2, t_1, t_2 and h are geometric parameters of the grid layer as illustrated in Fig. 2. E_1 and G_{12} are the longitudinal elastic and shear modulus of unidirectional composite materials of each layer. The transformed reduced stiffness matrix $[\bar{Q}]$ of the orthogrid layer is achieved by substituting $[Q]$ from Eq. (2) into Eq. (3).

$$[\bar{Q}] = [T]^{-1}[Q][T]^{-T} \tag{3}$$

where, $[T]$ is the transformation matrix [13] which is only depended on the grid orientation, θ, of each grid layer.

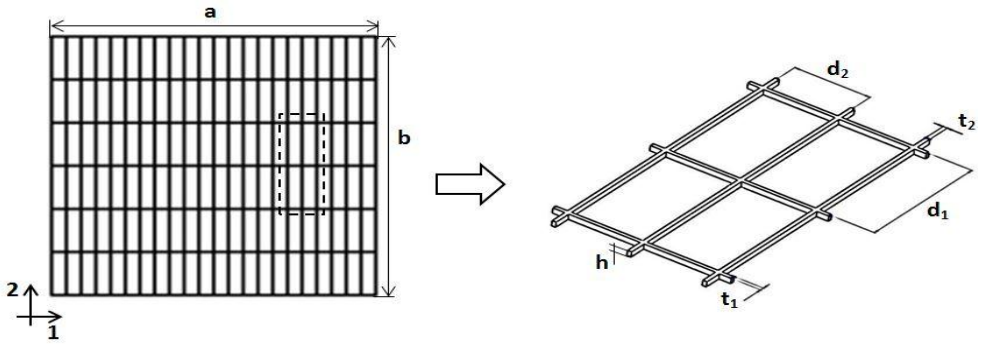

Fig.2
Geometries of conventional orthogrid.

3 NUMERICAL RESULTS AND DISCUSSION

Consider laminated grid plates that are composed of various numbers of similar conventional orthogrid layers. The total thickness of the plates is $H = N.h$, where, N is the number of layers and h is the thickness of each grid layer. It is assumed; the relative dimensions of a grid layer (see Fig. 2) are $a/b = 1,\ t_1/t_2 = 1.5,\ d_1/d_2 = 2$. The plates are made of various numbers of unidirectional carbon/epoxy orthogrid layers with the material properties which are presented in Table 1.

Table 1
Elastic properties of the Carbon/Epoxy composite material [14].

E_1	162×10^9 Pa
E_2	14.9×10^9 Pa
G_{12}	5.7×10^9 Pa
v_{12}	0.283
X_T	1744×10^6 Pa
X_C	1650×10^6 Pa
Y_T	52.6×10^6 Pa
Y_C	260×10^6 Pa
S	107.8×10^6 Pa

To investigate the effects of stacking sequences on the elements of the extensional and bending stiffness matrices ($[A]$ and $[D]$), two different cases of laminated grid plates are considered. The first configuration is $(\pm\theta)_{ns}$, that is achieved by repeating a specific sub-laminate $(\pm\theta)$ and called sub-laminate grid structure. The second case, which is called ply-level laminated grid, $(+\theta_m/-\theta_m)_s$, and is achieved by repeating each layer. Actually, a ply-level laminate is a special form of a sub-laminate with $n = 1$. These two laminated grid configurations are compared with a conventional orthogrid of the same dimensions. Table 2. presents the specifications of these three cases. The plates have equal thickness. Therefore, the weight of the cases remains the same.

Table 2
Properties of three different grid cases.

Case #	Configuration	Lay-up	Number of layers (N)	Each grid layer thickness (h)	a/b
1	Sub-laminate	$(\pm\theta)_{ns}, n = 2,...,5$	$4n$	$H/4n$	1
2	Ply-level	$(+\theta/-\theta)_s$	4	$H/4$	1
3	Orthogrid	(θ)	1	H	1

Based on the laminated plate theory, the force and moment resultants for a laminate are expressed as follows:

$$\tilde{N} = [A]\tilde{\varepsilon}_0 + [B]\tilde{\kappa}_0 \tag{4}$$

$$\tilde{M} = [B]\tilde{\varepsilon}_0 + [D]\tilde{\kappa}_0 \tag{5}$$

Since the response of the laminated structures subjected to an external cause depends on its stiffness, the variation of the elements of the stiffness can be used as a criterion. To show the effectiveness of the laminated grid over a conventional grid, the summations of the elements of the bending and extensional stiffness matrix of these two grids are used as a criterion. Moreover, two non-dimensional parameters, which illustrate the closeness of the laminate properties to the equivalent orthotropic layer, are used. To investigate the effects of the laminated grid stacking sequences on the extensional, $[A]$, and bending, $[D]$, stiffness matrices, the function "SUM" is

considered, which illustrates the summation of all elements of a matrix. Therefore, the summation for $[A]$ and $[D]$ matrices are defined as follows:

$$SUM(A) = \sum A_{ij} = A_{11} + A_{22} + A_{66} + 2(A_{12} + A_{16} + A_{26}) \tag{6}$$

$$SUM(D) = \sum D_{ij} = D_{11} + D_{22} + D_{66} + 2(D_{12} + D_{16} + D_{26}) \tag{7}$$

Moreover, two non-dimensional parameters, r_A and r_D, which are presented in Eqs.(8) and (9) define the variation of in-plane and out of plane property of a laminate from its equivalent orthotropic layer [15].

$$r_A = \sqrt{\left(\frac{A_{16}}{A_{11}}\right)^2 + \left(\frac{A_{26}}{A_{22}}\right)^2} \tag{8}$$

$$r_D = \sqrt{\left(\frac{D_{16}}{D_{11}}\right)^2 + \left(\frac{D_{26}}{D_{22}}\right)^2} \tag{9}$$

To evaluate the effects of grid orientation on the laminated grid stiffness matrices, the orientation of each grid lamina, θ, is varied from 0 to 90 degrees. Fig. 3 presents the variation of non-dimensional shear-extension coupling elements ($\bar{A}_{16}$ and $\bar{A}_{26}$) of the orthogrid and laminated grids. The overbar sign, $\bar{(\ )}$, shows the non-dimensional value of the parameter. The non-dimensional stiffness is defined by dividing each element of the extensional stiffness matrix by A_{22} of the specially orthogrid $(\theta = 0^\circ), \bar{A}_{ij} = A_{ij} / A_{22(\theta=0)}$.

As it can be seen in Fig. 3, the shear-extension elements of ply-level and sub-laminate grids are zero in contradiction with the orthogrid plate. $\bar{A}_{16}$ and $\bar{A}_{26}$ elements in orthogrid layer are negative and have the minimum values at $\theta = 60^\circ$ and $\theta = 30^\circ$, respectively.

Figs. 4 and 5 illustrate the variation of SUM$(\bar{A})$ and r_A for laminated grids and their corresponding orthogrid plate. The variation of SUM$(\bar{A})$ in the Fig. 4 can be explained according to Fig. 3. From Fig. 3, $\bar{A}_{16}$ and $\bar{A}_{26}$ elements are equal to zero for laminated grids and they have a negative value for the orthogrid. As shown in Fig. 4, the variation of the SUM$(\bar{A})$ for the laminated grids is completely different compare to orthogrid. For the orthogrid the maximum value of this summation is occurred at $\theta = 0^\circ$ and 90° with a minimum value at $\theta = 45^\circ$. However, for the laminated grids this summation is always larger than those of orthogrids and has a maximum at the grid orientation angle of 45 degree.

According to Fig. 3, there are no shear-extension couplings in laminated grids, and consequently, the r_A will be equal to zero as shown in Fig. 5. As depicted in Fig. 5 the laminated grid is closer to an equivalent orthogrid layer than corresponding conventional grid.

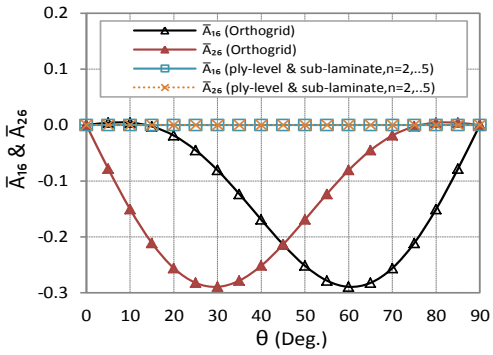

Fig.3
Comparison of non-dimensional shear-extension couplings for different cases as function of θ.

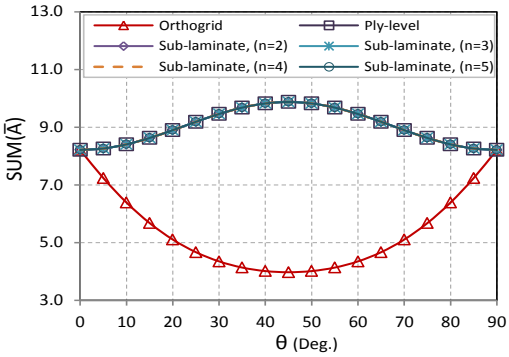

Fig.4
Comparison of SUM ($\bar{A}$) for the conventional orthogrids and laminated grids.

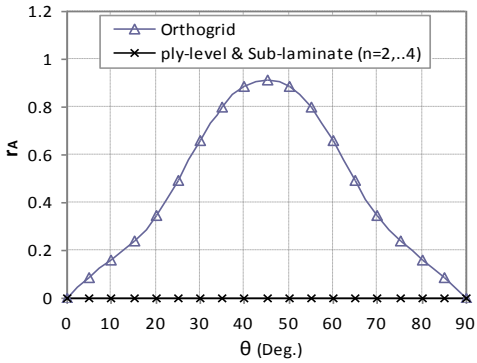

Fig.5
Non-dimensional parameter r_A for the different cases

Fig. 6 illustrates the variation of non-dimensional bending-twisting coupling ($\bar{D}_{16}$ and $\bar{D}_{26}$) elements for the presented cases. Due to symmetric behavior of the $\bar{D}_{16}$ and $\bar{D}_{26}$ graphs with respect to $\theta = 45^{\circ}$, only $\bar{D}_{16}$ graphs are shown in Fig. 6. For the orthogrid plate both $\bar{D}_{16}$ and $\bar{D}_{26}$ graphs are presented. Similar to the extension stiffness matrix, the non-dimensional elements are defined as $\bar{D}_{ij} = \bar{D}_{ij} / D_{22}$ which D_{22} is evaluated at $\theta = 0^{\circ}$.

As shown in Fig. 6, the orthogrid plate presents the largest negative bending-twisting coupling for most of the grid orientations. However, in the sub-laminate grid this coupling reduces and converges to a minimum value as the number of layers increases.

Fig. 7 illustrates the SUM ($\bar{D}$) for the presented grid configurations. For sub-laminate with $n \succ 2$, the summation reaches its maximum value at $\theta = 45$. The SUM ($\bar{D}$) value is reduced by decreasing the number of layers in the laminated grid. This behavior can be explained by reconsidering Fig. 6, which indicates the reduction of $\bar{D}_{16}$ and $\bar{D}_{26}$ when the number of layers increases.

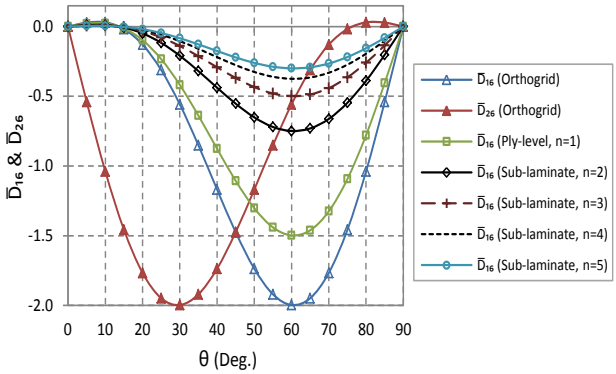

Fig.6
Non-dimensional Bending-Twisting couplings ($\bar{D}_{16}$ and $\bar{D}_{26}$) for the defined cases.

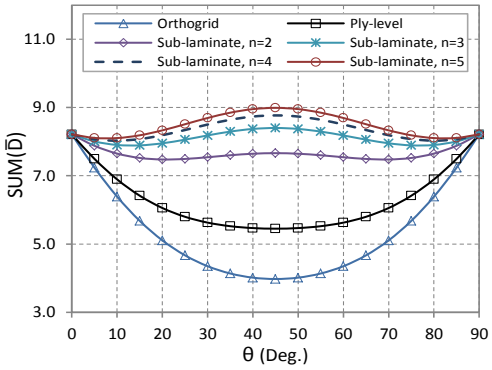

Fig.7
Comparison of SUM ($\bar{D}$) for the presented grid configurations.

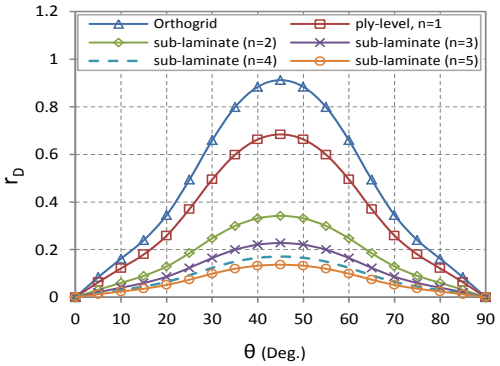

Fig.8
Variations of the non-dimensional parameter r_D for the different cases.

Fig. 8 shows the variation of the r_D parameter for different grid structures. As illustrated in Fig. 8, increasing the number of layers in the angle ply laminated grid reduces the r_D, which indicates the closeness of these laminated grids to behavior of a specially orthotropic layer.

In this section, the effects of different laminated grid configurations on the elements and the summation of the extension and bending stiffness matrices of symmetric laminated grid are presented. To illustrate these effects on a typical response of a laminated grid plate, in the next sections bending and failure behaviors of these three grid configurations are compared.

4 BENDING OF THE LAMINATED GRID PLATES

To examine the advantages of using laminated grid plates over conventional grid plates, the bending behavior of the defined cases are compared. Consider a square simply supported laminated grid plates subjected to a uniform transverse load. The Rayleigh-Ritz method is applied to achieve the maximum deflection of the plates. The total potential energy of the symmetric angle ply laminated grid plate subjected to lateral load can be expressed by the following equation [13]:

$$\pi = \Omega + U \tag{10}$$

where, U is the strain energy of bending and can be obtained from Eq. (11), and Ω is the potential of external forces.

$$U = \frac{1}{2}\int_0^b\int_0^a \left[D_{11}\left(\frac{\partial^2 w}{\partial x^2}\right)^2 + 2D_{12}\frac{\partial^2 w}{\partial x^2}\frac{\partial^2 w}{\partial y^2} + D_{22}\left(\frac{\partial^2 w}{\partial y^2}\right)^2 + 4D_{16}\frac{\partial^2 w}{\partial x^2}\frac{\partial^2 w}{\partial x\,\partial y} + 4D_{26}\frac{\partial^2 w}{\partial y^2}\frac{\partial^2 w}{\partial x\,\partial y} + 4D_{66}\left(\frac{\partial^2 w}{\partial x\,\partial y}\right)^2 \right] dx\,dy \tag{11}$$

For a lateral load p (per unit area) the potential of external force is given by

$$\Omega = \int_0^b \int_0^a [pw]dxdy \tag{12}$$

Similar to the isotropic plate, the following trigonometric function satisfies the geometric boundary conditions,

$$w(x,y) = \sum_{m=1}^{M}\sum_{n=1}^{N} W_{mn} \sin\frac{m\pi x}{a}\sin\frac{n\pi y}{b} \tag{13}$$

where, W_{mn} are arbitrary unknown coefficients. Substituting $w(x,y)$ from Eq. (13) in Eqs. (11, 12) and minimizing total energy from Eq. (10) with respect to the unknown W_{mn} coefficients, $M \times N$ linear and simultaneous equations will be produced:

$$\frac{\partial(\Omega + U)}{W_{mn}} = 0 \tag{14}$$

W_{mn} are calculated by solving these simultaneous equations. In Fig. 9 the non-dimensional maximum deflections of the laminated grids for different grid layer orientations, θ, compared with those of conventional orthogrids. The non-dimensional form of maximum deflection is defined as $\overline{W}_{max} = W_{max}/W_{max(orthogrid,\theta=0)}$.

To ensure the accuracy of the solution method, finite element model of the orthogrid and ply-level laminated grid plates are created in ABAQUS software and the non-dimensional maximum deflections of the plates are presented in Fig. 9.

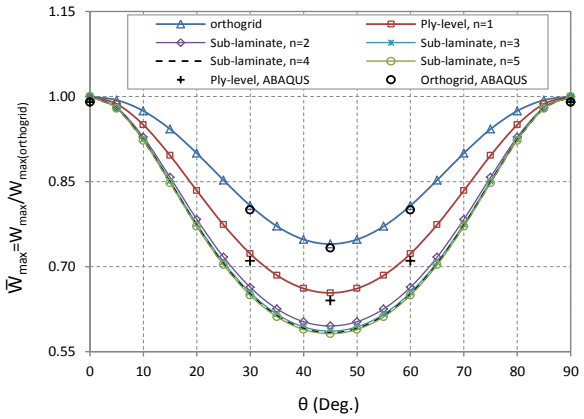

Fig.9
Non-dimensional maximum deflection for all cases under uniform lateral load.

As illustrated in Fig. 9, the minimum values of $\overline{W}_{max}$ for all cases are achieved at $\theta = 45^\circ$. Moreover, the sub-laminate with $n = 5$ which has the maximum SUM $(\bar{D})$ and minimum r_D, has the minimum deflection under lateral load. The deflection of the other sub-laminate cases, $n = 2,3,4$, except for $n = 1$, are also very close to sub-laminate with $n = 5$. Obviously, there is significant difference between response of the orthogrid and presented laminated gird. Clearly, using a laminated grid $((\pm\theta)_{5s})$ yields to 25% reduction in maximum deflection in comparison to the orthogrid (θ) with identical geometry and weight. This point proves the effectiveness of laminated grids over the conventional grids. To clarify the correlation between maximum deflection, and stiffness parameters, SUM $(\bar{D})$ and r_D, the variation of these parameters for orthogrid, and laminated grids are presented in Fig. 10 at $\theta = 45^\circ$. As demonstrated in the figure, when the number of layers increase in the laminated grid, the deflection and r_D decrease while, SUM $(\bar{D})$ increases compare to an orthogrid plate.

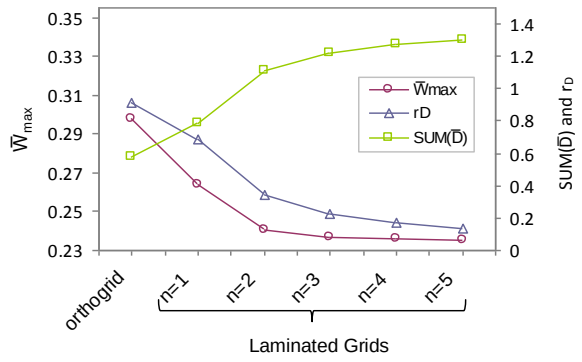

Fig.10
Variation of the W_{max} and stiffness parameters r_D and SUM $(\bar{D})$ for different cases at $\theta = 45^{\circ}$.

5 PROGRESSIVE FAILURE ANALYSIS

The presented results show that the bending response of the laminated grids is enhanced in comparison to conventional grids. However, due to angular position of the grid layers, the contact areas between the layers in the laminated grids are less than the conventional grids, which could increase the probability of the failure in the laminated grids.

To study the failure probability of the laminated grid plates, a progressive failure analysis has been conducted. This analysis considers the degradation of the material properties due to the failure of each element. Three principal failure modes have been considered in the present work; matrix failure, fiber-matrix shear failure and fiber failure. Table 3. presents these failure criteria [16,17].

Table 3
Applied failure criteria [16, 17].

Failure Mode	Failure Index	
Matrix tensile failure (σ_2>0)	$e_m^2 = \left(\frac{\sigma_2}{Y_T}\right)^2 + \frac{2\tau_{12}^2/G_{12} + 3\alpha\tau_{12}^4}{2S_c^2/G_{12} + 3\alpha S_c^4}$	(15)
Matrix compression failure (σ_2<0)	$e_m^2 = \left(\frac{\sigma_2}{Y_C}\right)^2 + \frac{2\tau_{12}^2/G_{12} + 3\alpha\tau_{12}^4}{2S_c^2/G_{12} + 3\alpha S_c^4}$	(16)
Fiber-matrix shear failure (σ_1<0)	$e_{fs}^2 = \left(\frac{\sigma_1}{X_C}\right)^2 + \frac{2\tau_{12}^2/G_{12} + 3\alpha\tau_{12}^4}{2S_c^2/G_{12} + 3\alpha S_c^4}$	(17)
Fiber tensile failure (σ_1>0)	$e_{fs}^2 = \left(\frac{\sigma_1}{X_T}\right)^2 + \frac{2\tau_{12}^2/G_{12} + 3\alpha\tau_{12}^4}{2S_c^2/G_{12} + 3\alpha S_c^4}$	(18)
Fiber compression failure (σ_1<0)	$e_f^2 = \left(\frac{\sigma_1}{X_C}\right)^2$	(19)

where σ_1, σ_2 and τ_{12} are the in-plane stress in the material coordinate system and α is a coefficient that is determined experimentally. To apply the progressive failure analysis in ABAQUS, the user subroutine modulus (USDFLD) is employed.

The subroutine is written in FORTRAN and is called by ABAQUS during analysis. In this method, three field variables are defined to indicate various failure modes and elastic properties are defined based on these variables. The first field variable (FV1) indicates the matrix failure mode. The second (FV2) presents fiber-matrix shearing failure, and the third (FV3) indicates fiber failure. The values of FV1-FV3 are equal to zero at the beginning of the analysis. When a failure index reaches to 1.0, the corresponding field variable sets equal to 1.0 and material properties degrade according to Table 4. The degradation model presented in [18] is applied in the current study.

Table 4
Correlation between material properties and field variables [18].

No failure	Matrix failure	Fiber-Matrix shear	Fiber failure
E_{11}	E_{11}	E_{11}	$E_{11} \to 0$
E_{22}	$E_{22} \to 0$	E_{22}	$E_{22} \to 0$
v_{12}	$v_{12} \to 0$	$v_{12} \to 0$	$v_{12} \to 0$
G_{12}	G_{12}	$G_{12} \to 0$	$G_{12} \to 0$
$FV\,1 = 0$	$FV\,1 = 1$	$FV\,1 = 0$	$FV\,1 = 1$
$FV\,2 = 0$	$FV\,2 = 0$	$FV\,2 = 1$	$FV\,2 = 1$
$FV\,3 = 0$	$FV\,3 = 0$	$FV\,3 = 0$	$FV\,3 = 1$

To analyze and compare the failure behavior of laminated and conventional grid, three grid plates are considered. The first plate is a conventional orthogrid (special orthogrid) layer at $\theta = 0^\circ$. The second is a conventional orthogrid (general orthogrid) layer at $\theta = 45^\circ$ and the third is a ply-level laminated grid at $(\theta = \pm 45^\circ)_S$. The grid dimensions are similar to cases investigated in previous section. The finite element models of these cases are shown in Fig. 11. The plates are simply supported along four edges and subjected to a uniform lateral load. The models are discretized by linear quadrilateral four-node elements [19]. The uniform lateral pressure is increased gradually on the plates, and failure behavior is studied during loading.

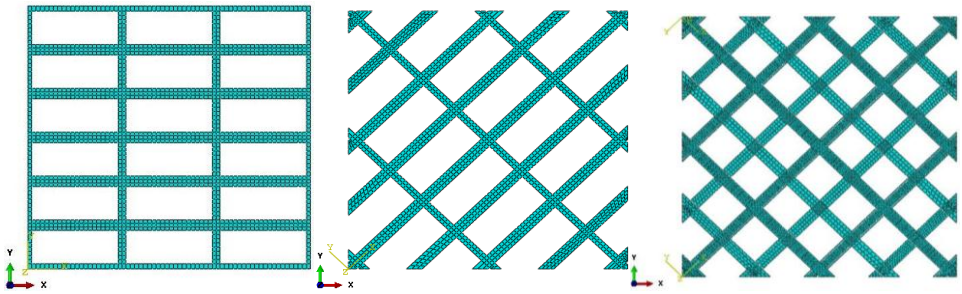

Fig.11
Finite element models for orthogrid plate at $\theta = 0^\circ$ (left), orthogrid plate at $\theta = 45^\circ$ (middle) and ply-level plate at $(\theta = \pm 45^\circ)_S$ (right).

Using USDFLD subroutine, the variation of different failure indices and their corresponding load are obtained. For each failure mode, the variations of the failure index of the plates are plotted for different applied load. Fig. 12 shows the maximum fiber failure index of three plates at different loads.

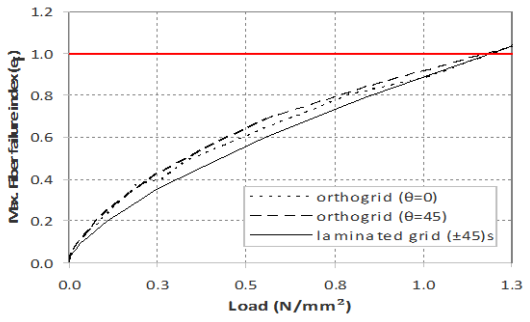

Fig.12
Max. Fiber failure index (e_f) for different lateral load.

As can be seen, all the samples are reached to critical index, 1.0, at the same load. On the other hand, the e_f for laminated grid is lower than two other conventional grids. Therefore, using laminated grid instead of conventional grid does not have adverse effects on the fiber failure of the plates. The Fig. 13 also illustrates the maximum fiber-matrix shear failure index of the plates for different loads.

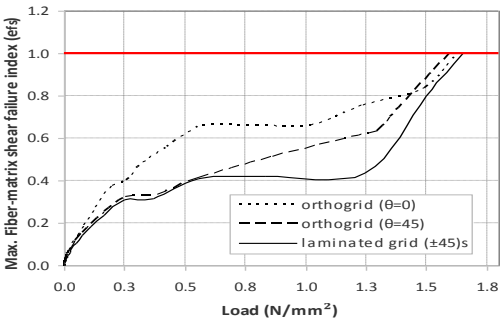

Fig.13
Max. Fiber-matrix shear failure index (e_{fs}) for different lateral load.

As the Fig. 13 shows, in different loads, the laminated grid has the minimum fiber-matrix shear failure. The plates have different shear failure indices for load less than 1.5 (N/mm^2). However, when the load increases, the plates failed $(e_{fs}=1)$ at a similar load. In Fig. 14 the maximum matrix failure index for different lateral load is presented.

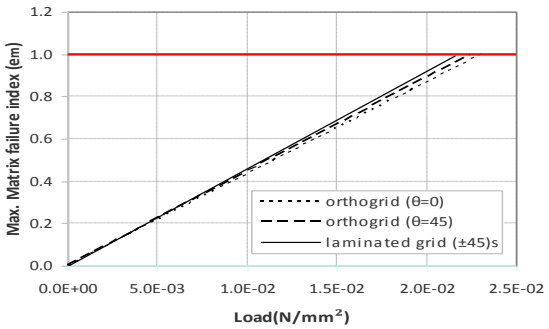

Fig.14
Max. Matrix failure index (e_m) for different lateral load.

According to Fig. 14, although all plates show a similar behavior, the orthogrid at $\theta=0$, failed at higher load. As it was expected, the laminated grid has slightly higher e_m compare to conventional grids. The general orthogrid $(\theta\neq 0)$ also has higher e_m compare to special orthogrid $(\theta=0)$. Results indicate that utilizing laminated grids instead of conventional grid, has no adverse effect on failure behavior of composite grid plates under lateral load.

6 CONCLUSIONS

In this study, the simple concept of laminated grid structures is introduced and the advantages of these structures over conventional grids are investigated. So far, a known grid structure such as orthogrid or isogrid is employed as an orthotropic layer. The present laminated grid is composed of various numbers of thin composite grid layers which its stiffness can be adjusted by choosing proper stacking sequences. Therefore, tailored stiffness of the structure can be achieved by using full anisotropic properties of the laminated grid. This concept yields to a large variety of laminated grid configurations with different coupling effects compare to conventional grids.

To investigate the advantages of the laminated grids, the stiffness of the laminated and conventional grids are compared and the response of the structures under lateral load is studied. The results show, choosing proper stacking sequences for the laminated grid changes the stiffness of the plates due to reduction of the twisting-bending and shear-extension couplings. As a result, the maximum deflection of the laminated grid considerably reduced in comparison with conventional grid.

Due to angular position of the grid layers, the contact area between the layers in the laminated grids is less than the conventional grids, which could increase the probability of the failure in the laminated grids. A failure analysis is performed using USDFLD subroutine in ABAQUS to compare the fiber, matrix and fiber-matrix shear failure modes of conventional and laminated grids. Results indicate the laminated and conventional grid plates have similar behavior in three principal failure modes. Therefore, using laminated grid as an alternative to conventional grid does not have adverse effects on the failure of the plates subject to a uniform lateral load.

REFERENCES

[1] Huybrechts S.M., Hahn S.E., Meink T.E., 1999, Grid stiffened structures: survey of fabrication, analysis and design methods, *Proceedings of the 12th International Conference on Composite Materials (ICCM/12)*.

[2] Chen H.J., Tsai S.W., 1996, Analysis and optimum design of composite grid structures, *Journal of Composite Materials* **30**: 503-534.

[3] Gürdal Z., Gendron G., 1993, Optimal design of geodesically stiffened composite cylindrical shells, *Composites Engineering* **3**: 1131-1147.

[4] Oliveira J.G., Christopoulos D.A., 1981, A practical method for the minimum weight design of stiffened plates under uniform lateral pressure, *Computers & Structures* **14**: 409-421.

[5] Kidane S., Li G., Helms J., Pang S.S., Woldesenbet E., 2003, Buckling load analysis of grid stiffened composite cylinders, *Composites Part B: Engineering* **34**: 1-9.

[6] Ambur D.R., Jaunky N., 2001, Optimal design of grid-stiffened panels and shells with variable curvature, *Composite Structures* **52**: 173-180.

[7] Chen C.J., Liu W., Chern S.M., 1994, Vibration analysis of stiffened plates, *Computers & Structures* **50**: 471-480.

[8] Shi S., Sun Z., Ren M., Chen H., Hu X., 2013, Buckling resistance of grid-stiffened carbon-fiber thin-shell structures, *Composites Part B: Engineering* **45**: 888-896.

[9] Lai C., Wang J., Liu C., 2014, Parameterized finite element modeling and buckling analysis of six typical composite grid cylindrical shells, *Applied Composite Materials* **21**: 739-758.

[10] Huang L., Sheikh A.H., Ng C. T., Griffith M.C., 2015, An efficient finite element model for buckling analysis of grid stiffened laminated composite plates, *Composite Structures* **122**: 41-50.

[11] Anyfantis K.N. , Tsouvalis N.G., 2012, Post buckling progressive failure analysis of composite laminated stiffened panels, *Applied Composite Materials* **19**: 219-236.

[12] Pietropaoli E., 2012, Progressive failure analysis of composite structures using a constitutive material model (USERMAT) developed and implemented in ANSYS, *Applied Composite Materials* **19**: 657-668.

[13] Kollar L.P., Springer G.S., 2003, *Mechanics of Composite Structures*, Cambridge University Press.

[14] Naik N.K., Chandra Sekher Y., Meduri S., 2000, Damage in woven-fabric composites subjected to low-velocity impact, *Composites Science and Technology* **60**: 731-744.

[15] Barbero E.J., 1999, *Introduction to Composite Materials Design*, Taylor & Francis.

[16] Chang F. K., Chang K.Y., 1987, A progressive damage model for laminated composites containing stress concentrations, *Journal of Composite Materials* **21**: 834-855.

[17] Lessard L.B., Shokrieh M.M., 1995, Two-dimensional modeling of composite pinned-joint failure, *Journal of Composite Materials* **29**: 671-697.

[18] Ambur D.R., Jaunky N., Hilburger M.W., 2004, Progressive failure studies of stiffened panels subjected to shear loading, *Composite Structures* **65**: 129-142.